11th International Symposium on Turbulence and Shear Flow Phenomena (TSFP11)
Southampton, UK, July 30 to August 2, 2019

CONTRIBUTION OF REYNOLDS-STRESS STRUCTURES TO THE SECONDARY FLOW IN TURBULENT DUCTS

Marco Atzori
Linné FLOW Centre
KTH Mechanics
SE-100 44 Stockholm, Sweden
atzori@mech.kth.se

Ricardo Vinuesa
Linné FLOW Centre
KTH Mechanics
SE-100 44 Stockholm, Sweden
rvinuesa@mech.kth.se

Adrián Lozano-Durán
Center for Turbulence Research (CTR)
Stanford University
Stanford, CA, USA
adrianld@stanford.edu

Philipp Schlatter
Linné FLOW Centre
KTH Mechanics
SE-100 44 Stockholm, Sweden
pschlatt@mech.kth.se

ABSTRACT

The present work is aimed at evaluating the contribution to the secondary flow in duct flow with square and rectangular cross section from three-dimensional coherent structures, defined as intense Reynolds-stress events. The contribution to a certain mean quantity is defined as the ensemble average over the detected coherent structures, weighted with their own occupied volume fraction. Our analysis unveils that the contribution to the cross-stream components of the mean velocity is either very similar to the same contribution in channel flow, or almost negligible in respect to the contribution from the portion of the domain not occupied by coherent structures. These results suggest that the most intense events are not directly responsible for the secondary flow.

INTRODUCTION

Mean properties of internal turbulent flows, such as skin friction and effective diffusivity, play an important role in numerous industrial and biological processes. Although the study of canonical flows such as periodic channel and circular pipe provide insights on the universal laws which govern wall-bounded flows, realistic cases do not exhibit periodicity in either the streamwise or the spanwise direction and therefore display more complex phenomena. An interesting example is the secondary flow of Prandtl's second kind, which arises in turbulent flows if both cross-stream directions are not homogeneous (Prandtl, 1926), *e.g.* in square and rectangular duct. Gavrilakis (1992) performed the first direct numerical simulation (DNS) on the square duct and several others authors followed up to the current time, providing a precise characterization of the Reynolds-number effects up to mean $Re_\tau^* = 1{,}000$ (Pirozzoli *et al.*, 2018). Note that the mean friction Reynolds number is defined as $Re_\tau^* = hu_\tau^*/\nu$, where h is the half height of the duct, u_τ^* is the friction velocity averaged over the perimeter and ν the kinematic viscosity. At moderate Reynolds number, the mean flow in the duct is significantly affected by the preferential locations of low- and high-speed streaks in the near-wall region. In particular, this results in a characteristic spanwise development of the wall-shear stress, which reflects the number of streaks contained in the domain (Pinelli *et al.*, 2010). As the Reynolds number increases, the wall-shear stress becomes more uniform in the center region, and the topology of the mean cross-stream components of the velocity becomes more complex. According to Gavrilakis (2019), this evolution leads to qualitatively changes of the mean flow up to $Re_\tau^* \approx 300$ and at larger Reynolds number it is possible to distinguish between a near-corner region and a core region. In the first, the mean velocity scales if it is expressed in outer units and the wall distance is in inner units, while in the latter it scales in outer units (Pinelli *et al.*, 2010; Pirozzoli *et al.*, 2018). The multiscale nature of the secondary flow makes a not trivial task to identify its origin and various hypotheses have been formulated. Based on the quadrant analysis performed on DNS results, Huser & Biringen (1993) conjectured that the secondary flow "can be explained by the preferred location of ejection structures [...] and interaction between burst events." However, Gavrilakis (2019) pointed out that the existence of an inflection point in the mean streamwise velocity suggests that the corner circulation is due to instability, while turbulence is responsible for the core circulation.

In the present work we study the relation between the secondary flow and instantaneous coherent structures. The structures are defined as proposed by Lozano-Durán *et al.* (2012), who studied the connected regions of the flow that fulfilled the condition for intense events in the spirit of the quadrant analysis (Wallace *et al.*, 1972). We perform a direct comparison between channel, square duct and rectangular duct, with two correlated aims: 1) characterizing how the different geometries affect the contributions from intense events to the mean cross-stream components of the velocity, and 2) investigating what is the role of such events in the process that originates the secondary flow of Prandtl's second kind.

DATA SET

In the present work we consider turbulent flow in square and rectangular duct with aspect ratio $AR = 3$ at $Re_\tau = 180$ and $Re_\tau = 360$ at the centre-plane. Note that the aspect ratio AR is defined as the ratio of lengths of the horizontal and the vertical walls and the friction Reynolds number Re_τ is computed with u_τ at the center-plane of the duct. This data set is part of that described by Vinuesa *et al.* (2018), who performed DNS with the spectral-element code *Nek5000* (Fisher *et al.*, 2008). A new data-set of turbulent channel flow, similar to that described by del Álamo *et al.* (2006) at the same friction Reynolds numbers is considered for comparison. Figure 1 shows the mean of the vertical and horizontal components of the velocity, V and W respectively, for the square and the rectangular duct. Here the bulk velocity and the half width of the duct h are employed to scale the velocity components and the spatial coordinates, respectively, and the origin of the reference frame is located at the bottom left corner with respect to the main flow direction. In order to identify the region of the flow for which it is meaningful to compare the different cases, we examine in detail the Reynolds-number and geometry effects on the secondary flow. We focus on the position of local extrema of the mean cross-stream components of the velocity in the bottom-left quadrant of the duct. In the square duct, the coordinates of the first maximum ($y^+ \simeq 77; z^+ = 11$) and of the first minimum ($y^+ = 50; z^+ = 50$) of V scale in inner units. Here x, y and z are the streamwise, wall-normal and spanwise coordinates, and the superscript + denotes inner scaling (either with u_τ or with ν/u_τ. The fact that the secondary flow is still evolving in this range of Reynolds numbers appears in the position of the second maximum of V, which does not scale either in inner or in outer units. Furthermore, a third maximum arises at $Re_\tau = 360$ at the center-plane, which is not present at $Re_\tau = 180$. In the rectangular duct the secondary flow extends through the domain in the horizontal direction and Reynolds-number and geometry effects are clearly distinguishable, although the geometry has also an impact on the scaling properties of the secondary flow. In fact, the corner circulation is confined closer to the wall when the Reynolds number increases, as in the square duct, but the location of the extrema of V and W does not scale in inner units in the rectangular duct. For instance, the location of the first maximum of V is ($y^+ = 71; z^+ = 11$) for $Re_\tau = 180$, but ($y^+ = 90; z^+ = 13$) for $Re_\tau = 360$. In addition, in the rectangular duct V and W become qualitatively different. The maximum of V associated with the core circulation is located at a distance from the vertical wall which is larger than the width of the square duct and other local maxima appear while approaching the vertical center-plane. However, V is positive almost always in the core region, and therefore the flow moves on average from the wall to the horizontal center-plane. On the other hand, W in the rectangular duct exhibits a change of sign along the horizontal center-plane, followed by a (negative) local minimum, and it approaches again 0 at the center of the duct ($y = 1; z = 3$) from a negative value. Therefore, along the horizontal axis the flow moves from the wall toward the center up to a certain distance from the vertical wall, but in the opposite direction at farther distance. Note that in the square duct V (or W) is always positive along the center-plane and gradually decreases to become 0 at the center ($y = 1; z = 1$). It is also interesting to observe that the position of the change of sign ($y = 1; z \simeq 0.5$) and of the local minimum ($y = 1; z \simeq 1.1$) do not depend on the Reynolds number, despite the fact that the evolution that W exhibits from $Re_\tau = 180$ to $Re_\tau = 360$ in the spanwise portion of the domain $z < 0.5$ is similar to that in the corresponding half of the domain in the square duct.

COHERENT STRUCTURE ANALYSIS

The detection of coherent structures follows the same procedure as in the study by Lozano-Durán *et al.* (2012) in turbulent channel flow, who performed a three-dimensional quadrant analysis and employed the percolation analysis to characterise the effect of the thresholds on the detected structures (as introduced by Moisy & Jiménez (2004)). These events are defined as connected regions of the domain which fulfill the condition $|uv| > H u_{\rm rms} v_{\rm rms}$, where u and v are the fluctuations with respect to the mean U and V of the streamwise and vertical component of the velocity, respectively, and H_{uv} is the considered threshold. Lozano-Durán *et al.* (2012) reported that intense uv events detected with $H = 2.0$ are responsible for $\approx 60\%$ of the Reynolds stress, despite occupying only $\approx 8\%$ of the volume of the domain. In duct flows, uv events play the role of uw events near vertical walls (and viceversa), and the presence of relatively large structures attached to two perpendicular walls makes this distinction not always meaningful. Therefore, in this work we consider coherent structured defined according to the conditions:

$$|uv| > H u_{\rm rms} v_{\rm rms} \quad \text{and} \quad |uw| > H u_{\rm rms} w_{\rm rms} \,. \qquad (1)$$

Preliminary results for the square duct at $Re_\tau = 180$, including the percolation analysis and a description of the geometrical properties of different families of objects classified based on the wall distance, have been recently reported by Atzori *et al.* (2018). The percolation analysis for uv and uw in the considered cases is shown in Figure 2. In this analysis we report the ratio between the volume of the largest structure $P_{\rm max}$ and the volume of all the structures $P_{\rm all}$ detected for a given threshold H. At low values of H the structures are merged into very large objects and $P_{\rm max}/P_{\rm all} \approx 1$, while for high values of H the intense events are isolated in more numerous but smaller structures and $P_{\rm max}/P_{\rm all} \ll 1$. The maximum slope of the curve $P_{\rm max}/P_{\rm all}$ identifies the *critical* value of H, for which the splitting process is more intense. In the square duct, the curves for uv and uw are in good agreement, which is expected because of the symmetry of the domain, whereas in the rectangular duct the critical value of H is lower for uw. The results for channel flow show that the relation between uv and uw is similar to that in the rectangular duct, although the percolation crisis is sharper and it has a weaker dependence on the Reynolds number. The differences in the percolation diagrams are probably due in part to the geometry of the domain and in part to structural differences in the turbulence fluctuations but here we do not investigated these effects in detail. Instead, we focus on the fractional contributions of intense events to the cross-stream components of the velocity. We denote the fractional contribution from a certain intense event XX to a mean quantity Ξ with the notation $\Xi^{>}_{\rm XX}$, while $\Xi^{<}_{\rm XX}$ is the fractional contributions from the complementary portion of the domain that does not belong to the events XX. For instance, $V^{>}_{uv}$ is the fractional contribution to the vertical component of the velocity from intense uv,

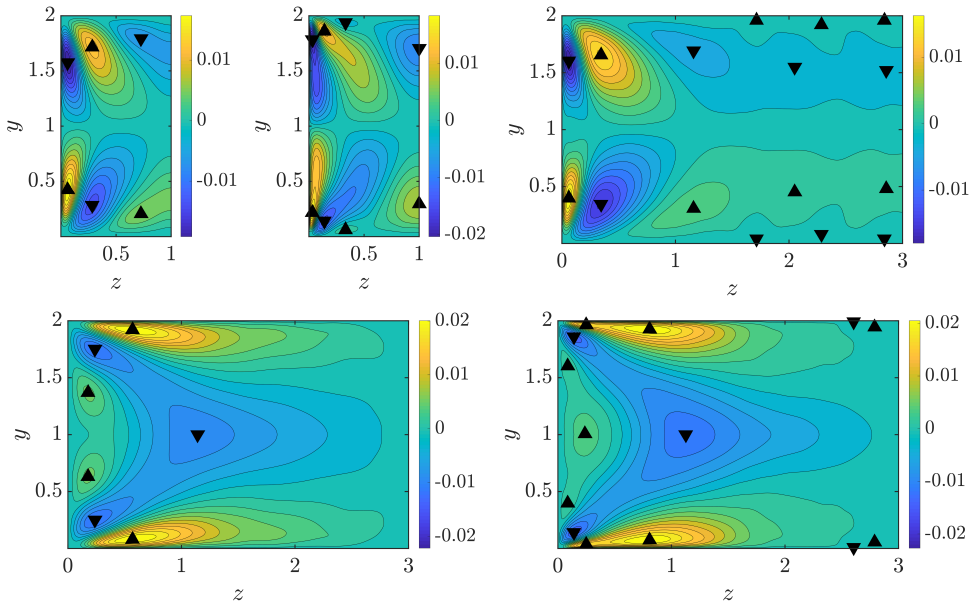

Figure 1. (Top) Vertical mean velocity component, V, for half of the domain in (from left to right) square duct at $Re_\tau = 180$, square duct at $Re_\tau = 360$ and rectangular duct with aspect ratio 3 at $Re_\tau = 180$. (Bottom) Horizontal mean velocity component, W, for half of the domain in rectangular duct at (left) $Re_\tau = 180$ and (right) $Re_\tau = 360$. Local maxima and local minima are indicated with upward and downward triangles, respectively.

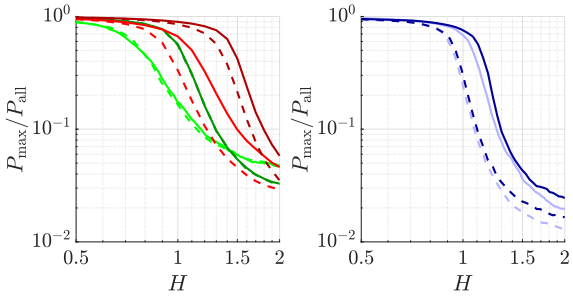

Figure 2. Percolation diagram for uv and uw events, denoted with solid and dashed lines, respectively. Square duct, rectangular duct and channel are in red, green and blue, respectively. Light colors are for $Re_\tau = 180$ and dark colors are for $Re_\tau = 360$.

which for a single field of the duct is computed as:

$$V_{uv}^{>}(j,k) = \frac{\sum_{i=1}^{N_x} p(i,j,k)}{N_x} \sum_{i=1}^{N_x} p(i,j,k)\, v'(i,j,k)\,, \qquad (2)$$

where i, j and k are the indices for the streamwise, vertical and spanwise directions, respectively, N_x is the number of grid points in the streamwise direction, $p(i,j,k)$ is 1 if $|uv(i,j,k)| > H_{uv} u_{\mathrm{rms}} v_{\mathrm{rms}}(j,k)$ and 0 otherwise, and v' is the value of the instantaneous vertical component of the velocity. Similarly, $V_{uv}^{<}$ is computed as:

$$V_{uv}^{<}(j,k) = \frac{\sum_{i=1}^{N_x} q(i,j,k)}{N_x} \sum_{i=1}^{N_x} q(i,j,k)\, v'(i,j,k)\,, \qquad (3)$$

where $q(i,j,k) = 1 - p(i,j,k)$. It follows immediately from the definitions above that $V = V_{uv}^{>} + V_{uv}^{<}$. It is worth stressing that $V_{uv}^{>}$ reflects both the intensity and the probability of occurrence of the considered events and thus the behaviour of $V_{uv}^{>}$ as a function of H_{uv} is not trivial.

RESULTS

We firstly consider the fractional contribution to the vertical component of the velocity in the channel and at the vertical center-plane of the duct from intense uv events, denoted by $V_{uv}^{>}$ (Figure 3). Since the fractional contributions are based on the ensemble average over the data-set, we report in Figure 3 both the time average of V and the corresponding ensemble average over the data-set, in order to provide an estimate of the statistical uncertainty. Furthermore, we compared the results obtained with the entire data-set and half of it, and the results do not change qualitatively (not shown here). The dependence of the intensity of the contribution on H is not monotonic in neither the channel nor the duct: in the channel (where $V = 0$), as H_{uv} increases up to $H_{uv} \simeq 2$, the absolute value of $V_{uv}^{>}$ also increases, but for higher H_{uv} the absolute value of $V_{uv}^{>}$ decreases. The duct exhibits a more complex behaviour because of the presence of the secondary flow. In fact, in the region where the secondary flow is weaker, $V_{uv}^{>}$ is higher than V for a certain range of H_{uv}, and in this case the dependence of $V_{uv}^{>}$ has the same non-monotonic behaviour as in the channel. On the other hand, where the secondary flow is stronger, $V_{uv}^{>}$ decreases monotonically as H_{uv} increases. However, in this work we do not study the dependence on the contributions on H_{uv}, but we focus on the comparison between channel and duct for $H_{uv} = 2.0$. Such H_{uv} is always higher than the critical one at which the percolation crisis occurs and therefore the most intense events are effectively isolated from the rest of the flow. In Figure 3 it is possible to appreciate the differences in the mean secondary flow for the various cases at this location, which are due to both aspect-ratio and Reynolds-number effects for $Re_\tau = 180$. In the core of the channel, $V_{uv}^{>}$ reflects the predominance of ejections among intense events, a result which was already re-

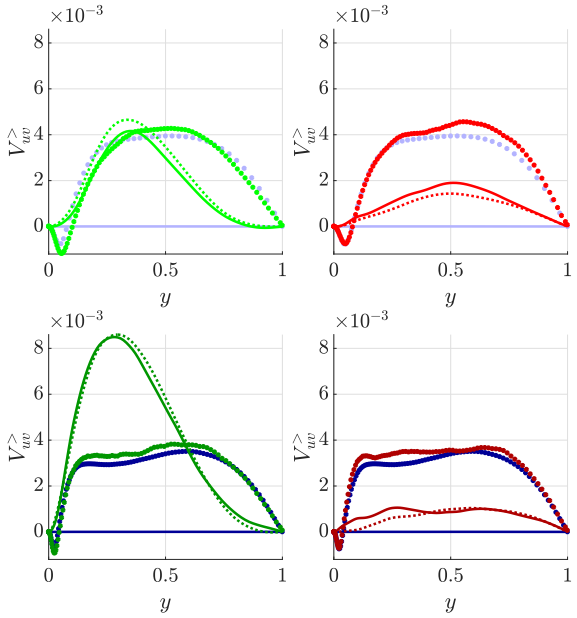

Figure 3. Vertical profile of (symbols) fractional contribution from intense uv events ($H_{uv} = 2$) to the vertical component of the velocity $V_{uv}^{>}$, compared with the (solid lines) ensemble average and (dotted lines) time average of the same component, V. Channel in blue; square and rectangular duct at the vertical center-plane in green and red, respectively. Light and dark colors are for $Re_\tau = 180$ and $Re_\tau = 360$, respectively.

ported at higher Re by Lozano-Durán *et al.* (2012). From the value of 0 at the wall, $V_{uv}^{>}$ initially decreases reaching a minimum at $y^+ \simeq 9$ before increasing farther from the wall and it changes sign at $y^+ \simeq 15$. For $y^+ > 15$, it further increases reaching an almost constant value at $y^+ \simeq 50$, before decreasing again above $y \simeq 0.60$ to become 0 along the horizontal center-plane. The first change of sign of $V_{uv}^{>}$ coincides with the transition between the viscous wall region, where the most intense fluctuations are the consequence of sweeps that occur farther from the wall, and the logarithmic region, where ejection events in respect to the closer wall are predominant (this trend does not depend on the choice of H_{uv}). It is reasonable to conjecture that, closer to the horizontal center-plane of the channel, the largest ejection events from the opposite wall start to have an influence, eventually reaching a balance at $y/h = 1$. Despite the differences in the secondary flow, for all the cases considered here there is a good agreement between $V_{uv}^{>}$ for the channel and the duct. It is interesting to observe that such similarity is not affected by the differences in the relative intensity of the contribution $V_{uv}^{>}$ and the mean V. In fact, in the square duct at $Re_\tau = 360$, for which the center-plane is the location of a local maximum and the secondary flow is expected to scale in outer units, V is higher than $V_{uv}^{>}$ up to $y/h \approx 0.7$. In the square duct at $Re_\tau = 180$, the secondary flow is less intense and $V_{uv}^{>}$ is, by chance, in good agreement with V between $y^+ > 15$ and $y/h < 0.3$. In the rectangular duct, where the vertical center-plane is farther from the vertical wall and the secondary flow is relatively weak, V is almost always lower than $V_{uv}^{>}$.

As opposed to what happens at the vertical center-plane, $V_{uv}^{>}$ in the duct significantly differs to that in the channel in the near-corner region, where the secondary flow scales if the

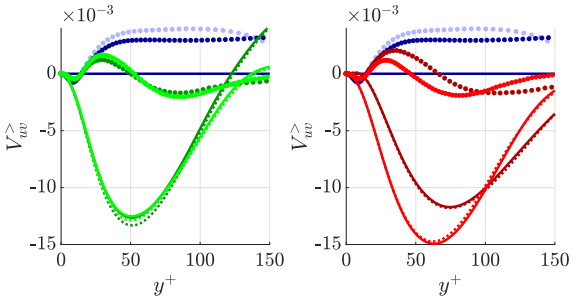

Figure 4. Vertical profiles of the fractional contribution $V_{uv}^{>}$ ($H_{uv} = 2$) in the channel and at the location of local minimum closer to corner in square and rectangular duct compared with the ensemble and time average. Colors and symbols as in Figure 3.

wall-normal distance is expressed in viscous units. Figure 4 shows $V_{uv}^{>}$ and V in the duct at the location of the minimum of V. The contribution in the channel is reported as well as a reference. At this location, V is negative, therefore its sign is opposite to that of $V_{uv}^{>}$ in the channel. However, above the near-wall region and below the corner bisector, *i.e.* $15 < y^+ < 50$ for the square duct, intense ejections are relevant enough to have $V_{uv}^{>}$ positive. Furthermore, in a relatively small region up to $y^+ \simeq 25$, including the near-wall region where intense sweeps are prevalent, $V_{uv}^{>}$ is in good agreement between channel and duct. Note that V in the square duct scales well up to $y^+ \approx 100$. Despite the fact that the behavior of V and of $V_{uv}^{>}$ as functions of the wall-normal distance are qualitatively different, the effect of the geometry in the rectangular duct is quite similar for both of them. In fact, in the square duct $V_{uv}^{>}$ scales if the wall-normal distance is expressed in inner units as V does, and the agreement of $V_{uv}^{>}$ between $Re_\tau = 180$ and $Re_\tau = 360$ is better for the square duct than for the channel. In the rectangular duct, $V_{uv}^{>}$ does not scale, as it happens for V, and the locations of the local extrema for both $V_{uv}^{>}$ and V move farther from the horizontal wall as the Reynolds number increases. To better characterize the evolution of the contribution $V_{uv}^{>}$, we consider its dependence on the distance from the vertical wall at a fixed distance from the horizontal wall equal to $y^+ = 50$ (Figure 5). The behaviour of $V_{uv}^{>}$ follows a common pattern for both Reynolds numbers, as well as for square and rectangular ducts and it is possible to identify three different regimes in terms of the distance from the vertical wall. In the near-corner region, where V scales in inner units, $V_{uv}^{>}$ also scales in inner units, although the position of the local extrema does not match with that of the V. In particular, the first local maximum and local minimum of $V_{uv}^{>}$ are closer to the vertical wall than the corresponding maximum and minimum of V. Farther from the vertical wall, it is possible to identify an intermediate region where $V_{uv}^{>}$ does not scale in inner units but it increases while approaching the value of $V_{uv}^{>}(y^+ = 50)$ in the channel at the same Reynolds number. In this intermediate span-wise region, the trend of $V_{uv}^{>}$ vaguely resembles that of V, in the sense if there is a certain range of z^+ where V is increasing (or decreasing) it is possible to identify a correspondent range of z^+, at lower distance from the vertical wall, where $V_{uv}^{>}$ is also increasing (or decreasing). For example, for both square and rectangular ducts at $Re_\tau = 180$, after V reaches the minimum at $z^+ \approx 50^+$ it increases up to a local maximum, which is higher than $V_{uv}^{>}$ in the channel, and it decreases again for

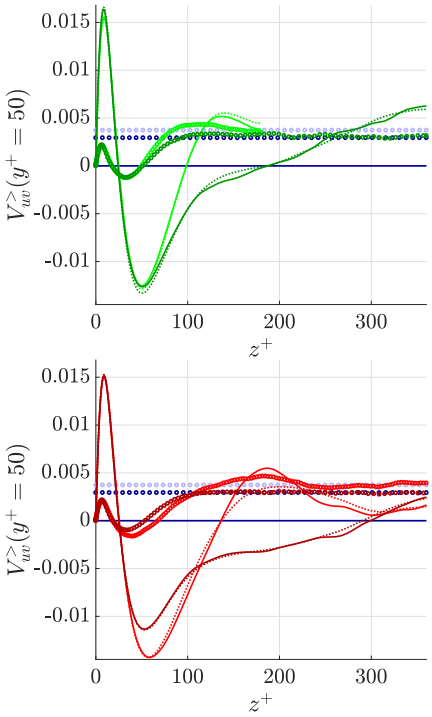

Figure 5. Horizontal profile at $y^+ = 50$ of the contribution $V_{uv}^{>}$ ($H_{uv} = 2$) for square and rectangular duct, compared with $V_{uv}^{>}(y^+ = 50)$ in the channel and the time and ensemble averages. Colors and symbols as in Figure 3.

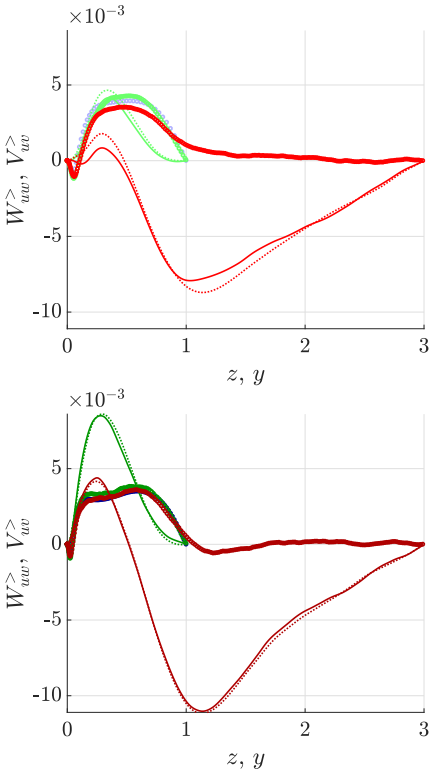

Figure 6. Contribution to the horizontal component of the velocity in square and rectangular ducts form intense uw events, $W_{uw}^{>}$, compared with the mean W and the contribution $V_{uv}^{>}$ in the channel. Colors and symbols as in Figure 3.

higher z^+. The contribution $V_{uv}^{>}$ has a similar trend, including a region where $V_{uv}^{>}$ in the duct is higher than $V_{uv}^{>}$ in the channel, but, as in the near-corner region, the local extrema have different positions. Even farther from the wall it is possible to identify a third spanwise region, for which $V_{uv}^{>}$ at $y^+ = 50$ approaches asymptotically the value of $V_{uv}^{>}$ for the same wall-normal distance in the channel. The extension of this region is very small for the square duct at $Re_\tau = 180$, for which it is limited at $z^+ > 160$, and for the rectangular duct at the same Reynolds number it appears at a distance from the wall higher than the half-height of the duct ($z^+ \simeq 220$). In this asymptotic region $V_{uv}^{<}$ is almost constant and it does not show any correlation with the secondary flow, despite the fact that the relatively amplitude of $V_{uv}^{<}$ and V changes with z^+ and it differs in the different cases. For instance, in the squared duct at $Re_\tau = 360$ the contribution $V_{uv}^{>}$ remains constant for $z^+ > 200$, *i.e.* the region where V monotonically increases from ≈ 0 to a value higher than that of $V_{uv}^{>}$ approaching the vertical center-plane.

In the square duct the two cross-stream components of the velocity are identical, together with the relative contributions, *e.g.* $V_{uw}^{>}$ and $W_{uw}^{>}$. On the other hand, as we have previously discussed, V and W are qualitatively different in the rectangular duct, due to the change of sing of W in the core region in the latter. Figure 6 shows, for both Reynolds numbers, the contributions to the horizontal component of the velocity from intense uw events, $W_{uw}^{>}$, and the contribution $V_{uv}^{>}$ in channel flow for comparison. The profiles are reported as functions of the wall-distance in outer units, *i.e.* the span-wise coordinate z for the rectangular duct ($0 < z < 3$) and for the square duct ($0 < z < 1$) and the vertical coordinate for the channel ($0 < y < 1$). At this location it is possible to clearly distinguish between geometry and Reynolds-number effects on W. On the one hand, the secondary motion is more intense for $Re_\tau = 360$ than for $Re_\tau = 180$, which is due to the fact that in the latter the core circulation is not present. On the other hand, for both Reynolds numbers, the maximum of W is lower in the rectangular duct, W changes sign at a similar distance from the vertical wall for both rectangular ducts ($z \simeq 0.5$) and it exhibits a minimum at a distance from the vertical wall higher than the half-height of the duct ($z \simeq 1.1$). However, both the Reynolds number and the geometry have a less significant impact on the contribution from the intense events $W_{uw}^{>}$. In fact, as observed for $V_{uv}^{>}$ along the vertical center-plane, $W_{uw}^{>}$ does not follow the span-wise dependence of W and it is in good agreement in channel, square and rectangular duct and in relatively good agreement in the duct at different Reynolds numbers, despite the presence of the secondary flow. Such agreement holds up to a distance from the vertical wall which is almost the half-height of the duct, and it is better for higher Reynolds. In particular, $W_{uw}^{>}$ exhibits for all the cases the change of sign at $z^+ \simeq 15$ and the same almost constant value of $V_{uv}^{>}$ above $z^+ \simeq 50$ ($W_{uw}^{>}$ is slightly lower in the rectangular duct than in the square duct, but these differences are within the statistical uncertainty). Furthermore, despite the fact that the vertical center-plane in the rectangular duct is at a distance from the wall three times larger than for channel flow, $W_{uw}^{>}$ decreases at a very similar distance from the wall of approximately $z \simeq 0.6$. The differences between $W_{uw}^{>}$ in the rectangular duct with respect to $W_{uw}^{>}$ (or $V_{uv}^{>}$) in the square duct and $V_{uv}^{>}$ in the channel are limited in how the first approach 0 at the center-plane, at $z/h = \simeq 0.6$. In the rectangular duct, $W_{uw}^{>}$ exhibits an inflection point and gradually reaches 0 farther from the wall. Interestingly, there is a qualitative difference between the

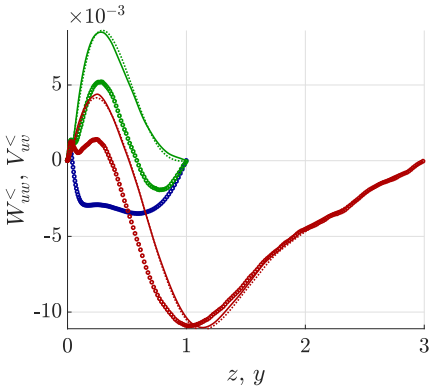

Figure 7. Contribution to the horizontal component of the velocity in square and rectangular duct from the portion of the domain complementary to intense uw events in the duct, $W_{uw}^{<}$, compared with the mean W and the corresponding contribution $V_{uv}^{<}$ in the channel. Colors and symbols as in Figure 3.

two considered Reynolds numbers, which may be related with the still evolving structure of the secondary flow. In fact, at $Re_\tau = 180$ the contribution remains always positive, while at $Re_\tau = 360$ it becomes negative right after $z = 1$, reaching again 0 from below closer to the vertical center plane. The distance from the wall and the spanwise evolution suggest that the process that gradually yields to $W_{uw}^{>}$ in the region $z > 1$ in the rectangular duct is fundamentally different from that occurring for $V_{uv}^{>}$ in channel and duct approaching the centre-plane.

We also examined the contributions to V and W from the complementary portion of the domain which does not belong to intense uv and uw events, denoted $V_{uv}^{<}$ and $W_{uw}^{<}$ respectively. Since the contribution from intense events are either unrelated to the secondary flow or negligible for the mean velocity, $V_{uv}^{<}$ and $W_{uw}^{<}$ exhibit the same qualitative behaviour as V and W. Thus, they differ significantly in duct and channel, as shown in Figure 7.

CONCLUSIONS

In the present work we have examined the fractional contributions of intense Reynolds-stress events to the secondary flow of Prandtl's second kind in duct with square or rectangular cross-section. The intense events are detected following the three-dimensional extension of the quadrant analysis introduced by Lozano-Durán *et al.* (2012), which studies the connected regions of the domain that fulfill a condition such as $|uv| > H_{uv} u_{\rm rms} v_{\rm rms}$ or $|uw| > H_{uw} u_{\rm rms} w_{\rm rms}$. The fractional contributions are computed as a weighted ensemble average over the corresponding portion of the domain occupied by the events. Considering the results of the percolation analysis for different thresholds, we focused on the results obtained for $H_{uv} = 2$ and $H_{uw} = 2$, which is a value high enough to assure that the most intense events are isolated. Our results show that the majority of intense events are not directly responsible for the secondary flow of Prandtl's second kind, although they are affected by it in certain regions of the domain. In particular, two different behaviours are observed, a fact that reflects the multi-scale nature of the secondary flow. In the core region, where the secondary flow scales in outer units, the contribution to V in duct flow is in good agreement with the same contribution in channel flow, regardless of the intensity of secondary flow. In the corner region, where the secondary flow scale if the distance from the wall is expressed in outer units, the fractional contributions are less intense than in the channel or in the core region, and almost everywhere much less intense than the contributions from the portion of the domain not included in the intense events. Furthermore, in rectangular ducts the Reynolds-stress events do not yield a noticeable contribution to the core circulation towards the vertical walls, which is characteristic of that flow. These observations suggest that the generation of the secondary flow cannot be explained directly in terms of the interactions between intense ejection and sweeps events, and that more complex phenomena need to be considered.

Acknowledgments

This study was funded by the Swedish Foundation for Strategic Research, project "In-Situ Big Data Analysis for Flow and Climate Simulations" (ref. number BD15-0082) and by the Knut and Alice Wallenberg Foundation. The simulations were performed on resources provided by the Swedish National Infrastructure for Computing (SNIC).

References

del Álamo, J.C., Jiménez, J., Zandonade, P. & Moser, R.D. 2006 Self-similar vortex cluster in the turbulent logarithmic region. *J. Fluid Mech.* **561**, 329–358.

Atzori, M., Vinuesa, R., Lozano-Durán, A. & Schlatter, P. 2018 Characterization of turbulent coherent structures in square duct flow. *J. Phys.: Conf. Ser.* **1001**, 012008.

Fisher, P.F., Kruse, J., Mullen, J., Tufo, H., Lottes, J. & Kerkemeier, S. 2008 Nek5000: open source spectral element cfd solver. Available at `http://nek5000.mcs.anl.gov/`.

Gavrilakis, S. 1992 Numerical simulation of low-reynolds-number turbulent flow through a straight square duct. *J. Fluid Mech.* **244**, 101–129.

Gavrilakis, S. 2019 Post-transitional periodic flow in a straight square duct. *J. Fluid Mech.* **859**, 731–753.

Huser, A. & Biringen, S. 1993 Direct numerical simulation of turbulent flow in a square duct. *J. Fluid Mech.* **257**, 65–95.

Lozano-Durán, A., Flores, O. & Jiménez, J. 2012 The three-dimensional structure of momentum transfer in turbulent channels. *J. Fluid Mech.* **694**, 100–130.

Moisy, F. & Jiménez, J. 2004 Geometry and clustering of intense structures in isotropic turbulence. *J. Fluid Mech.* **513**, 111–133.

Pinelli, A., Uhlmann, M., Sekimoto, A. & Kawahara, G. 2010 Reynolds number dependence of mean flow structures in square duct turbulence. *J. Fluid Mech.* **644**, 107–122.

Pirozzoli, S., Modesti, D., Orlandi, P. & Grasso, F. 2018 Turbulence and secondary motions in square duct flow. *J. Fluid Mech.* **840**, 631–655.

Prandtl, L. 1926 Über die ausgebildete Turbulenz. *Verh. 2nd Int. Kong. für Tech. Mech., Zürich.* Transl. *NACA Tech. Memo* 435, pp. 62–75.

Vinuesa, R., Schlatter, P. & Nagib, H. M. 2018 Secondary flow in turbulent ducts with increasing aspect ratio. *Phys. Rev. Fluids* **3**, 054606.

Wallace, J. M., Eckelman, H. & Brodkey, R. S. 1972 The wall region in turbulent shear flow. *J. Fluid Mech.* **54**, 39–48.